Investigation of the structural properties of calcium aluminosilicate slags with varying Al_2O_3/SiO_2 ratios using molecular dynamics

Kai Zheng[1)], Zuotai Zhang[1)], Feihua Yang[2)] and Seetharaman Sridhar[3)]

1) *Department of Energy and Resources Engineering, College of Engineering, Peking University, 100871, Beijng, P.R.China*
2) *Beijing Building Materials Academy of Sciences Research, 100041, Beijing, P.R.China*
3) *Department of Materials Science and Engineering, Carnegie Mellon University, Pittsburgh, PA, USA*

Abstract: Molecular dynamics simulation was explored to investigate the change of structure of calcium aluminosilicate slags with varying Al_2O_3/ SiO_2 ratios at a fixed CaO content. In practice the results of the study are relevant to the significant changes in slag structure caused by the changes in chemical composition during continuous casting of steels containing high amounts of dissolved aluminum. It was found that Q^4 tetrahedral species (tetrahedron with four bridging oxygens) increased while NBOs (non-bridging oxygen) decreased with increasing Al_2O_3/SiO_2 mole ratio, suggesting that a more polymerized network was formed. The concentration of oxygen tricluster increased dramatically up to 24% with increasing Al_2O_3/SiO_2 mole ratio. The coordination number for Al (CN_{Al-O}) was also observed to increase from 4.02 for sample CAS1 to 4.11 for sample CAS11, suggesting that high coordination number of Al presents in the slag melt with the substitution of [AlO_4] for [SiO_4]. NBOs prefer to be coordinated with Si and Al tends to be localized in more polymerized environment as network intermediate phases. The degree of Al avoidance was calculated and the Al avoidance principle is applicable in the SiO_2 rich regions.

Keywords: Molecular dynamics, calcium aluminosilicate slag, slag structure, Al_2O_3/SiO_2 ratio

1. Introduction

Aluminosilicate glasses and melts are not only among the major constituents of Earth's mantle and crust but also play a significant role in industrial process such as glass and ceramic manufacture, ironmaking and steelmaking. Among them the calcium aluminosilicate (CAS) ternary system is particularly attractive. For instance, CAS glasses have been applied extensively by virtue of their excellent optical, mechanical properties and their refractory features, and the ternary melts is also the main compositions of slag used in ironmaking and steelmaking processes. It is well known that the macroscopic physical and chemical properties of CAS system is determined by the structure, i.e. the size of the charged polymeric units that comprise the melt and it is therefore important to acquire the structure's atomic-scale information. This has been studied through various sorts of techniques e.g. Nuclear Magnetic Resonance (NMR) [1-4)], X-Ray absorption spectroscopy (XAS) [5,6)], neutron diffraction [7,8)], Raman scattering [9,10)] and molecular dynamics (MD) simulation [11-14)]. However, previous studies mainly paid their attention to CAS glasses or slags with a low silica mole fraction or a varying CaO proportion. How the structure changes with varying Al_2O_3/SiO_2 ratio has not been investigated so far.

In recent years, high strength steels such as Transformation Induced Plasticity (TRIP) steel or Twining Induced Plasticity (TWIP) steels et.al have drawn wide attentions because of its lightweight automotive applications. The

additional Al in the steel is expected to react with the slags containing SiO_2 and the reaction increases the Al_2O_3/SiO_2 ratio during the casting process, causing great process control problems and significant changes in structural and thermophysical properties. It is well known that the [SiO_4] and [AlO_4] tetrahedra in CAS system are the fundamental structural units, which are connected by sharing oxygen atoms to form a three-dimensional network and Ca atoms are dispersed in those networks. The charge deficiency of [AlO_4] tetrahedron must be compensated by Ca cations, i.e., Ca atoms may play the role of network modifier or charge balancing, depending on the CaO/Al_2O_3 ratio. Furthermore, the 'Al avoidance' principle has been debated in literature regarding its accuracy and the range of application. Structural defects such as non-bridging oxygen [12,15], tricluster [11,16,17,18] and Al^V [19,20,21] also occupy considerable quantities and have deep influences on the system's structure and properties. In this paper, MD (Molecular Dynamic) simulation is applied to the CAS slags at a fixed CaO content and various molar ratios between SiO_2 (64% to 24%) and Al_2O_3 (6% to 46%) to promote understanding the change of the primary structural properties with varying Al_2O_3/SiO_2 ratios, including partial radial distribution function (RDF), coordination number (CN), distributions of different types of oxygen, bond lengths and bond angles. These studies may provide clues to how to control or engineer slags used in casting high strength steels.

2. Simulation method

In the molecular dynamic simulations of aluminosilicate slags, the choice of a suitable potential function and its corresponding parameters is critical for the success of a simulation. There are several potential functions such as Born-Mayer-Higgins (BMH) and Stillinger-Weber (SW) potentials which were generally used during past years, and a pair atom potential function of BMH form which has been successfully used for CAS glasses or melts [11-13] was applied here:

$$U(r_{ij}) = \frac{q_i q_j}{r_{ij}} + A_{ij} \exp(-B_{ij} \cdot r_{ij}) \quad (1)$$

where $U(r_{ij})$ is the interatomic pair potential, q_i, q_j are the selected charges and r_{ij} denotes the distance between atoms i and j. The first term of right hand side corresponds to the Coulombic interaction, which can be calculated using the standard charge of each element. The second term represents inter-core short range repulsion interaction. A_{ij} and B_{ij} are adjustable parameters and the determined values are listed in **Table 1**. Those values have been proven successful in the simulation of aluminosilicate slags [13,19]. The Ewald method was used to calculate the Coulomb interaction for each atom and the cutoff of potential was 10Å when evaluating the repulsive forces.

Table 1 Parameters for the BMH potentials.

Atom1	Atom2	A_{ij}(eV)	B_{ij}(1/Å)
Ca	Ca	9684.976	3.448
Ca	Si	1362.401	4.492
Ca	Al	4879.785	3.448
Ca	O	3718.745	3.448
Si	Si	1.866×10^{19}	40.00
Si	Al	2219.246	3.448
Si	O	223440.540	7.018
Al	Al	2444.136	3.650
Al	O	1945.759	3.546
O	O	15812.842	3.846

As mentioned, the present simulation chooses the samples of the ternary system $CaO\text{-}SiO_2\text{-}Al_2O_3$ with varying Al_2O_3/SiO_2 mole ratio at a fixed mole ratio of CaO which is a simplification of a mold slag that is currently under trial in the steel industry for casting of TRIP steels [22]. The samples were divided into 11 groups with varying Al_2O_3/SiO_2 mole

ratio as shown in **Table 2**. The numbers of different atoms are then decided according to the mole fractions, given that the total number is about 4000. The density of every sample was calculated with a model proposed by Courtial and Dingwell [23]. Assuming that all 4000 atoms are put in a cubic model box, the molar mass and density together decide the length of box, which is also listed in **Table 2**.

Table 2 The composition of slag melts, atomic numbers, density and the length of model cubic box

Groups	Mole fraction			Atomic number					Density	Length/Å
	CaO	SiO2	Al_2O_3	Ca	Si	Al	O	total	g/cm^3	
CAS1	0.3	0.64	0.06	425	908	170	2496	3999	2.488	38.7320
CAS2	0.3	0.6	0.1	414	827	276	2482	3999	2.510	38.6067
CAS3	0.3	0.56	0.14	402	752	376	2470	4000	2.531	38.4876
CAS4	0.3	0.52	0.18	392	680	470	2457	3999	2.551	38.3728
CAS5	0.3	0.48	0.22	382	612	560	2446	4000	2.571	38.2645
CAS6	0.3	0.44	0.26	372	547	646	2435	4000	2.590	38.1587
CAS7	0.3	0.4	0.3	363	485	728	2425	4001	2.608	38.0635
CAS8	0.3	0.36	0.34	355	427	804	2415	4001	2.626	37.9677
CAS9	0.3	0.32	0.38	347	370	878	2404	3999	2.644	37.8666
CAS10	0.3	0.28	0.42	339	316	950	2396	4001	2.660	37.7872
CAS11	0.3	0.24	0.46	332	265	1016	2386	3999	2.677	37.6937

Since the number of atoms is always smaller than wanted due to the calculation resources, periodic boundary conditions are applied on all faces of the model box to create an infinite system with no boundaries. During the simulation the leap frog integration method was used and the initial velocities were drawn randomly from a Maxwell-Boltzmann distribution. Before the simulation process starts, four types of atoms with appropriate composition were placed randomly into the model box and equilibrated at 5000 K for 30000 time steps (the time for each step is 1 fs) to compose the initial configuration. Another type of initial configuration was composed by Metropolis Monte Carlo method. Subsequently, the sample was cooled down from 5000 K to 2000 K in steps of 500 K. During every step the relaxation of total potential energy was carried out for 20 ps. Then the temperature was fixed at 2000 K for another 30000 time steps, and the partial radial distribution functions (RDF) were therefore achieved and the balance conformations were collected to do the microscopic structure analysis during this period. We also performed another group of simulations whose simulated time in every step was only half of the previous one, and no significant difference was observed in the results of these two groups. So, the selected simulation method is feasible and the results are convincible. All simulations are performed in NVT ensemble (i.e. the volume and temperature of the samples are controlled) and carried out using Materials Explorer program (FUJITSU LIMITED).

3. Results and discussion

3.1 Radial distribution functions (RDF) and coordination numbers (CN)

The RDFs indicate the average number of atoms of atomic species *j* that are located at a distance r from a target atomic species *i* atoms and it is defined as follows,

$$g_{ij}(r) = \frac{V}{N_i N_j} \sum_{k}^{N_i} \frac{n_{kj}(r - \Delta r/2, r + \Delta r/2)}{4\pi r^2 \Delta r} \tag{2}$$

where N_i (N_j) is the total number of atomic species *i* (*j*) atoms included in the system, n_{kj} is the number of atomic species *k* atoms included in a spherical shell of thickness Δr located at a distance *r*, and *V* is the volume of the system. The RDFs not only describe the character of short-range order and long-range disorder of the slag melt, but also provide the basic structural information including the average bond lengths and average coordination numbers. The running CN is

calculated through integration of the corresponding RDF and the chosen cutoff is the position of the first valley of RDF.

$$N_{ij}(r) = \frac{4\pi N_j}{V}\int_0^r r^2 g_{ij}(r)\mathrm{d}r \qquad (3)$$

Figure 1 shows the curves of RDFs and running CNs for all atomic pairs of the sample CAS9 as an example. The first peaks of Si-O, Al-O and Ca-O RDFs, which correspond to the most probable bond distances, are equal to 1.60, 1.77 and 2.40Å, respectively. These are in agreement with the previous reports [7,13,24] that measured by an X-ray and neutron diffraction techniques or obtained through MD simulations using the SW potential function. It is also noted that the first peak of Si-O shows a narrow and sharp shape, suggesting that the [SiO_4] tetrahedron is very stable and the stable feature of [SiO_4] tetrahedron is partially inherited by [AlO_4] tetrahedral unit. The running CN also helps to promote an understanding the structural properties of the melts. For instance, the running $CN_{Si\text{-}O}$ occupies a smooth platform equal to 4 at the vertical axis, indicating that the overwhelming majority of Si atoms are 4-coodinated with oxygen. The curve of running $CN_{Al\text{-}O}$ also possesses a slanting platform, which indicates that the average $CN_{Al\text{-}O}$ is 4.10 for sample CAS9. This on one hand demonstrates that the Al tetrahedral unit is not as stable as the [SiO_4] tetrahedron, and on the other hand suggests that some high-coordinated Al units do exist in the CAS slags [11,15,16]. Ca in the system has no significant structure that is stable and the simulated results indicate that the running $CN_{Ca\text{-}O}$ is 7.02, which is a litter larger than the experimental results by XAS [25].

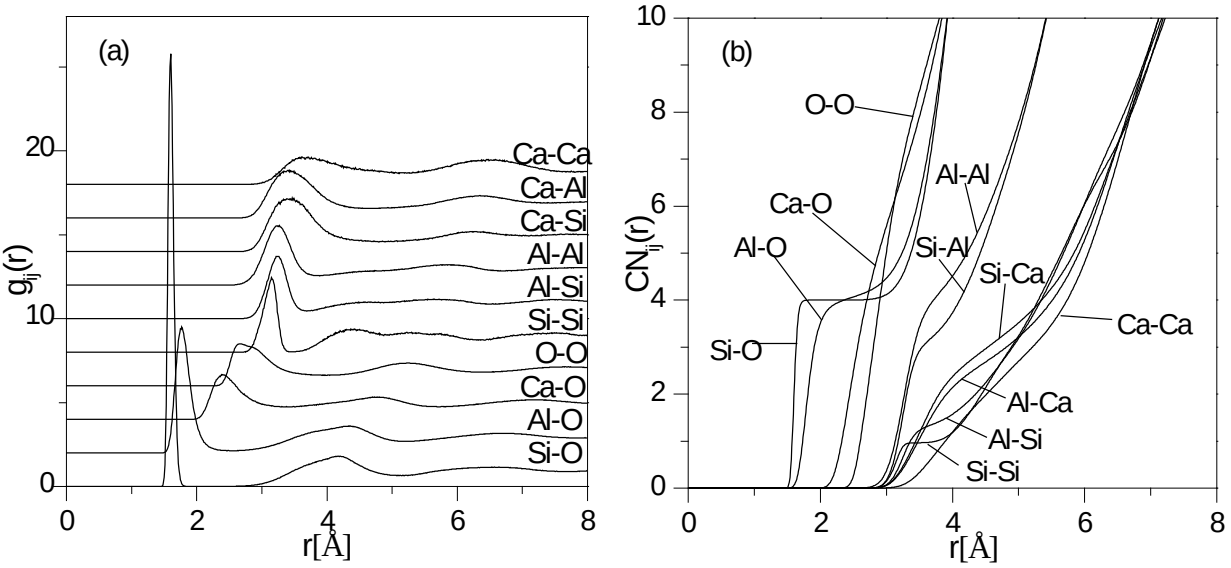

Figure 1 (a) The RDFs of simulation and **(b)** the running CNs of sample CAS9.

There is an interesting transformation of the first peak of O-O atomic pair, as shown in **Figure 2**, and the O-O peaks provide the detailed information about what is the major structural unit in the slags. In the SiO_2 rich region (CAS1 to CAS6), the first peak value equals to 2.61±0.01Å, corresponding to the typical distance between oxygen atoms in a [SiO_4] tetrahedron. While the value converts to 2.85Å in an Al_2O_3 rich region (CAS11), corresponding to the O-O distance in an [AlO_4] tetrahedron. The peculiar peak with an accompanying shoulder appears in the curve for sample CAS8 as the content of SiO_2 and Al_2O_3 is approximately equivalent, demonstrating that [AlO_4] units have already occupied a considerable part of the networks. Similar results were also reported by XAS [7] and the MD simulations for other slag systems [19].

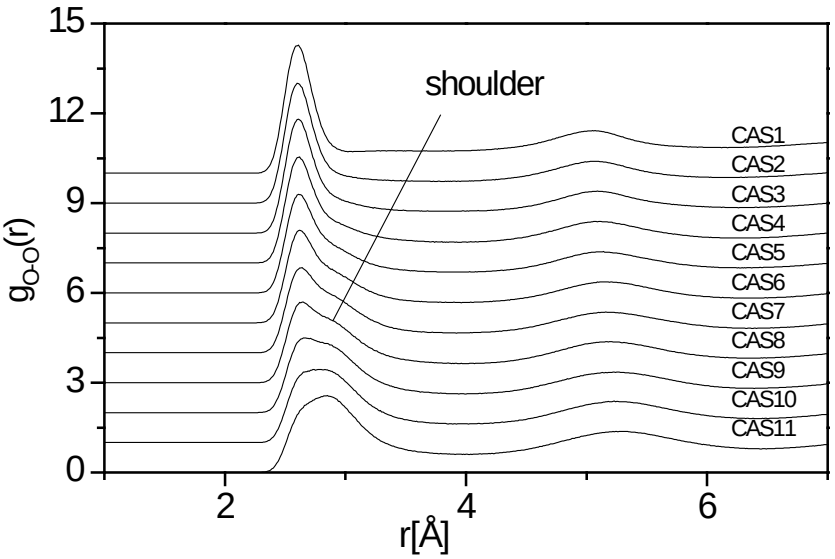

Figure 2 RDFs for O-O pairs of all CAS slags.

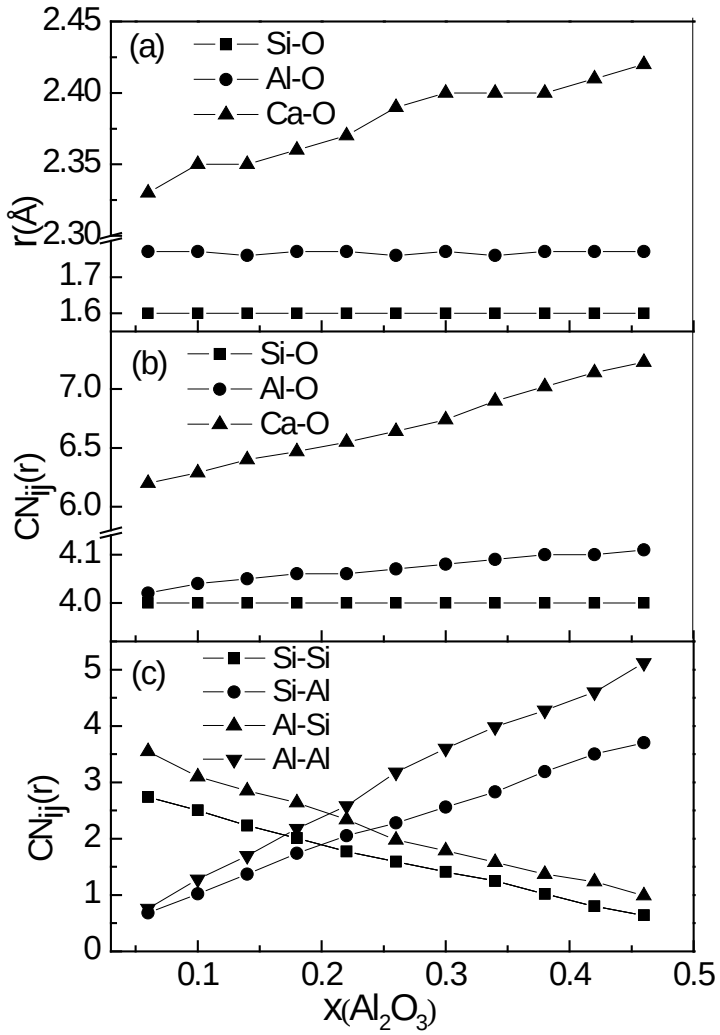

Figure 3 (a) The position of the first peak of RDFs, **(b)** coordination numbers of Si-O, Al-O and Ca-O, **(c)** coordination numbers of Si-Si, Si-Al, Al-Si and Al-Al as a function of mole fraction of Al_2O_3.

The variation of structural properties of CAS slags with composition was studied and the results were shown in **Figure 3**. It can be seen that the [SiO_4] tetrahedral unit has proven its high stability by the first peak's position (1.60Å) and coordination number (4.00) which keep constant with varying Al_2O_3/SiO_2 ratio. A small alteration is detected in CN_{Al-O} from 4.02 to 4.11, indicating that the Al^V or Al^{VI} units may appear and increases with an increasing Al_2O_3/SiO_2 ratio. It is interesting to note that the role of Ca changed from network modifiers to charge balancing, followed by a noticeable increase in both peak's position and coordination numbers. This may suggest that the average distance between Ca and tetrahedral units becomes bigger and Ca must provide charge compensating for more [AlO_4] units. Furthermore, the coordination numbers of next-nearest neighbors around the network-former cations are recorded in **Figure 3(c)**. Special attention should be paid that CN_{Si-Si} and CN_{Al-Al} reach the maximum for samples CAS1 (2.74) and CAS11 (5.12), respectively, and the latter is almost twice as much as the former even when the content of Al_2O_3 in sample CAS11 is smaller than that of SiO_2 in sample CAS1. This implies that Al is more likely to aggregate to form some more complicated structural units.

Therefore, it can be seen from above results that the [SiO_4] tetrahedral unit is very stable, and the microstructure change in CAS slag melt is mainly due to the amphoteric behavior of alumina. The simulation indicates that the running CN_{Al-O} increases from 4.02 to 4.11, suggesting that high coordination number of Al presents in the slag melt with the substitution of [AlO_4] for [SiO_4] and the role of Ca changes from network modifiers to charge balancing.

3.2 BOs, NBOs and oxygen triclusters

Before studying balance configurations out of final 30000 time steps, accurate coordinates of every atom in the cubic model box, as the fundamental factor of micro-structural analysis, were saved to calculate the distances between two atoms and angles shaped by three atoms and thereby to get the distribution of them. As shown in **Figure 1(a)**, the RDFs of Si-O and Al-O have their first valleys whose corresponding x-axis values are around 2.0 and 2.5Å respectively, meaning that in those radial ranges from Si or Al the probability of finding O atoms is very close to zero. The cutoff radius (2.0Å for Si and 2.5Å for Al) was therefore decided, where O atom was considered to be coordinated with Si or Al atom. According to this criterion, each O atom was marked as a specific type by the number of network-former atoms that it was coordinated with.

The numbers of BO, NBO and triclusters were counted using the aforementioned method and the results are presented in **Figure 4(a)**, where tricluster indicates that the oxygen atom is coordinated with three network formers. Free oxygens which link two network-modifiers (Ca-O-Ca) also appear in the system with a very small fraction (less than 0.2%), and this may be due to the fact that the Ca-O-Ca sites are energetically unstable and not able to exist for long. The proportion of NBOs falls remarkably from 28.5% to 5.9% with an increasing Al_2O_3/SiO_2 ratio, which is in conformity with the conventional concept that when the content of Ca exceeds that needed for charge compensating, T-O-T (T is Si or Al) linkages will be broken to form NBOs. Nevertheless, NBOs still hold a considerable percentage even when CaO/Al_2O_3 ratio is equal or less than 1, as many previous works have demonstrated [26,11]. Despite the small fraction, NBOs are divided into two groups, namely Ca-O_{nb}-Si and Ca-O_{nb}-Al, the relative constituents of which were figured out in **Table 3**. The conclusion can therefore be drawn that NBOs strongly prefer to be localized on Si. This is probably because that the [SiO_4] tetrahedral unit does not need the charge balancing, resulting in more Ca playing the role of network modifier,

cutting off Si-O-T linkages to form Si-O_{nb}-Ca, and the same consequence was acquired by the ^{17}O MAS NMR spectra [1] and high-energy x-ray diffraction [27]. This also indicates that Al is more likely to coordinate with BOs.

Figure 4(b) shows the varying tendency of relative contents of three types of BOs, that is Si-O-Si, Al-O-Al and Si-O-Al. The fractions of first two vary reasonably with increasing content of Al_2O_3, while Si-O-Al reaches the maximum of 0.50 for sample CAS6 when the number of Si atom is slightly larger than Al. To further reveal the relationship among three BO species, the interaction of them could be described by the reaction [1],

$$\text{Al-O-Al} + \text{Si-O-Si} \leftrightarrow 2(\text{Si-O-Al}) \quad (4)$$

The calculated equilibrium constant K_{BO} in the present simulation is 6.36±1.30. The so-called 'Al avoidance' principle put forward that Si-O-Al linkage is energetically more favorable than Al-O-Al and Si-O-Si linkages [28]. To examine the accuracy of this principle, the degree of 'Al avoidance' was estimated in samples CAS1 and CAS11 by calculating the proportion of numbers of Al-O-Al linkages to the theoretic Al-O-Al numbers, and the estimated proportions are 61.7% and 94.9% for sample CAS1 and sample CAS11, respectively. This suggests that Al avoidance rule is more effective in SiO_2-rich region. Similar results were observed by 3Q MAS NMR spectra [29] and MD simulations [12].

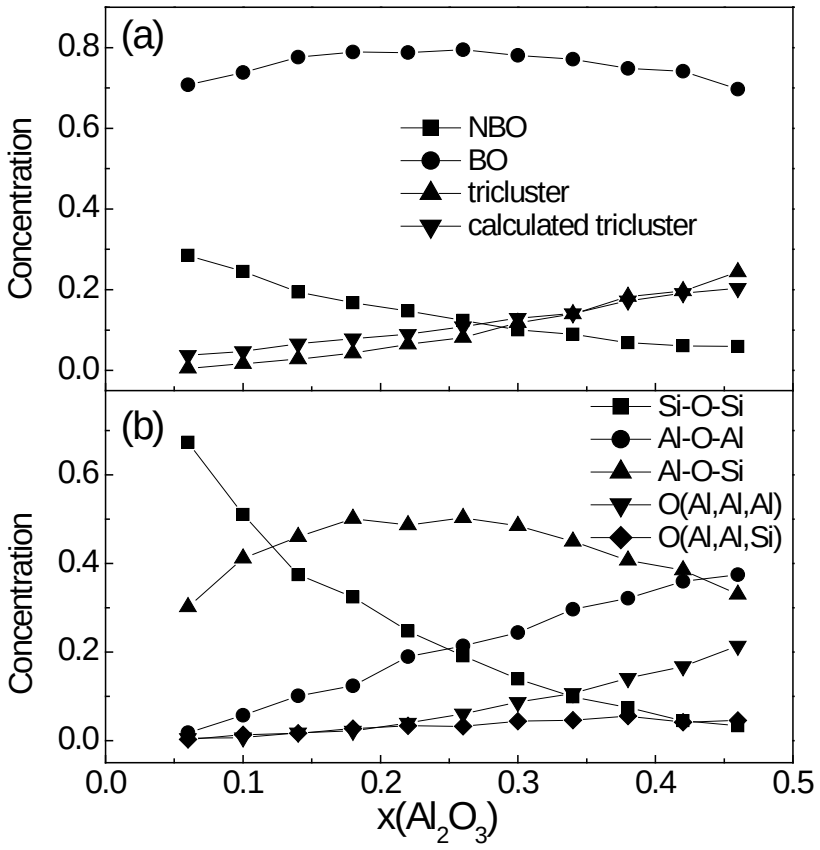

Figure 4 Concentration of different types of O as a function of mole fraction of Al_2O_3.

Table 3 Relative contents of Ca-O_{nb}-Si and Ca-O_{nb}-Al. The values are calculated by [Ca-O_{nb}-Si]/[SiO_2] and [Ca-O_{nb}-Al]/(2[Al_2O_3])

	CAS1	CAS3	CAS5	CAS7	CAS9	CAS11
NBO(Si)	0.422	0.313	0.243	0.186	0.146	0.142
NBO(Al)	0.124	0.068	0.070	0.043	0.029	0.028

The oxygen triclusters have been widely investigated about their existence [18,30], conformation [31], quantity [12,13] and influences on dynamics properties [11]. Number fractions of triclusters are traced and plotted in **Figure 4(a)** with a prominent increase from 0.5% to 24% with increasing Al_2O_3/SiO_2 ratio. A simple reaction $O^I + O^{III} \leftrightarrow 2O^{II}$ (O^I, O^{II} and O^{III} represent NBOs BOs and triclusters respectively) describing the transition process of three O species was proposed and the equilibrium constant $K_O = [O^{II}]^2/[O^I][O^{III}]$ (bracketed quantities refer to the number fractions of different O species) was equal to 49 in 2000K calculated by Morgan and Spera [20]. Thus the predicted concentration of O^{III} was achieved by K_O with $[O^{II}]$ as well as $[O^I]$ and displayed to compare with the simulated values. It can be seen that the calculated values are in agreement with simulated data. Oxygen triclusters are generally composed of O(Al, Al, Al), O(Al, Al, Si) and O(Al, Si, Si), and it is noted that the proportion of O(Al, Si, Si) is less than 0.5% and no O(Si, Si, Si) was observed (**Figure 4(b)**). This is probably because that triclusters play the role of charge compensating to $[AlO_4]$ tetrahedron, whereas $[SiO_4]$ tetrahedron is electrically neutral so that it is very difficult for the stable Si-O_b-Si site to be coordinated with a third cation to form O(Al, Si, Si) or O(Si, Si, Si). As shown in **Figure 5**, triclusters can also be treated as the corner shared by three tetrahedrons, two of which, mostly both $[AlO_4]$ tetrahedrons, have a certain probability to share an edge (O-O). But this edge-sharing phenomenon seems not applicable between $[SiO_4]$ and $[AlO_4]$, whose edges are unstable with each other and will undoubtedly give rise to structural distortion and a rapid energetic raise if edge-sharing occurs.

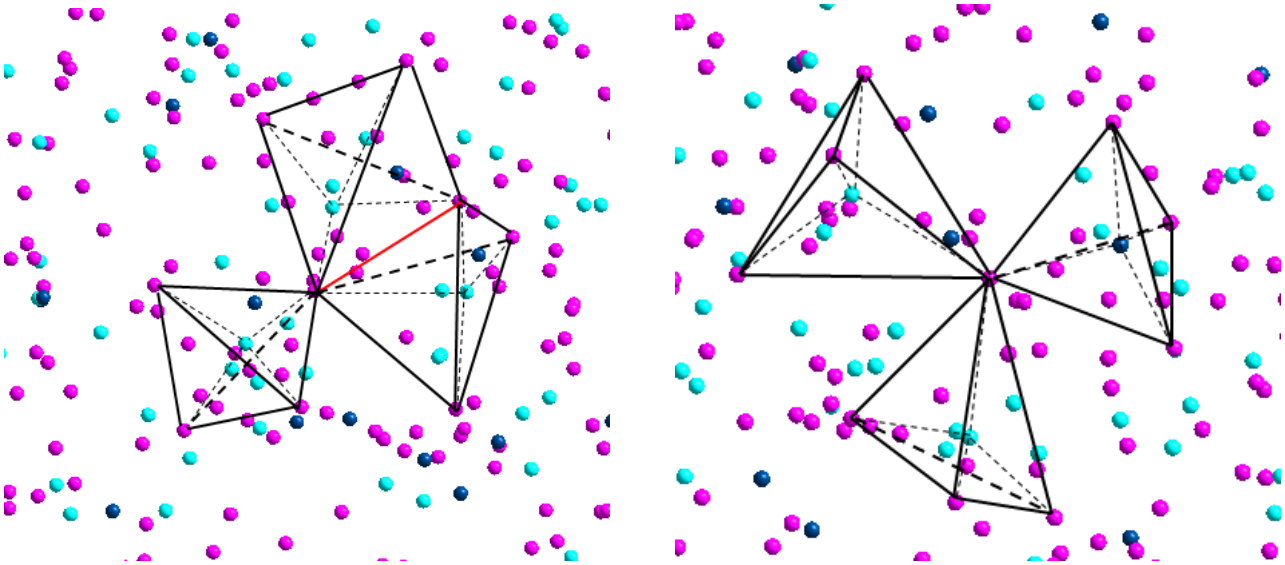

(a) (b)

Figure 5 Configurations of different types of oxygen triclusters. (a) The O atom shared by three AlO_4 tetrahedrons, two of which have a common edge; (b) the O atom shared by two AlO_4 tetrahedrons and one SiO_4. (Si, Al, O atoms are marked by balls with the color of deep blue, light blue and pink, respectively. Si (Al) tetrahedrons are outlined by thick lines and thin dash lines represent Si-O or Al-O bonds. Red line in (a) is the edge shared by two tetrahedrons).

In summary, the concentration of NBO decreases from 28.5% to 5.9% with increasing Al_2O_3/SiO_2 ratio and NBO prefers to be localized on Si. The degree of Al avoidance is applicable in SiO_2 rich region. An increasing Al_2O_3/SiO_2 ratio gives rise to oxygen triclusters which are mainly composed of O(Al, Al, Al) and O(Al, Al, Si).

3.3 Distributions of 5-coordinated Al and Q^n

Figure 6(a) illustrates the distribution of Al with different coordination number as a function of Al_2O_3 mole fraction. It should be noted that the concentration of Al^{IV} preponderates over others with a percentage more than 87%. The concentration of Al^V varies from 4% to 10% in an indistinct way with composition, and reaches the maximum as the SiO_2 content is 40 mol% corresponding to sample CAS7. Al^V increases dramatically from 5.5% to 9.4% in CAS6 and CAS7, and decreases slightly to 7.8% in CAS8. This irregular variation can be interpreted by the amphoteric character of Al. That is, the substitution of Al for Si gives rise to a change of the role of Al from an acid to an alkali. The separation line of the variation is CAS7, where the molar ratio Al_2O_3/CaO equals to 1. The ^{27}Al MAS NMR spectra [15] reported the similar fraction of Al^V (4% to 8.9%) in SiO_2-rich glasses. Another NMR experiment [16] and a molecular modeling study [11] reported that the concentration of Al^V exhibits a maximum value (7.2%) as the silica content is around 35 mol% at a fixed CaO/Al_2O_3 ratio equal to 1. The Al^{III} should also be taken notice of especially in the first five CAS slags with the fraction of 4%, where enough Ca cations are present to provide charge compensation of [AlO_4] tetrahedron. Meanwhile, Al^{VI} is barely observed in our samples (less than 0.3%) and is therefore not considered to be significant. Furthermore, taking the three types of oxygen into account, the formation of Al^V can be interpreted by three reactions [11],

$$Al^{IV} \leftrightarrow Al^{III} + O^{I} \quad (5a)$$

$$Al^{III} + O^{II} \leftrightarrow Al^{IV} + O^{III} \quad (5b)$$

$$Al^{IV} + O^{I} \leftrightarrow Al^{V} \quad (5b)$$

As the intermediate phase of reactions, Al^V and triclusters intensively affect the structural properties of CAS slags, such as self-diffusion coefficients.

Figure 6(b) and **(c)** elucidate the proportion of Q^n (n is the number of BO and oxygen tricluster in one tetrahedron) in [SiO_4] and [AlO_4] tetrahedral units shifting with Al_2O_3/SiO_2 ratio. It can be seen that the concentration of Q^4 increases dramatically at the cost of a decreasing in Q^2 and Q^3 and shares a similar variation trend with the total fraction of O^{II} and O^{III}. The degree of polymerization (DOP) can be measured by $(Q^4+Q^3)/(Q^2+Q^1)$ and therefore increases with Al_2O_3/SiO_2 ratio. This further indicates that the viscosity of CAS slags may increase as SiO_2 is replaced by Al_2O_3, for a given CaO content. Most available viscosity data [32,33] agree well with our conclusion. In the ternary slag systems of K_2O-Al_2O_3-SiO_2 at 1350 ℃, Na_2O-Al_2O_3-SiO_2 at 1500 ℃, CaO-Al_2O_3-SiO_2 at 1550 ℃ when the Al_2O_3/SiO_2 exceeds 0.4, the viscosity increases monotonically with the increase of Al_2O_3/SiO_2 molar ratio. But for CaO-Al_2O_3-SiO_2 slags at 1550 ℃, the viscosity increases with increasing Al_2O_3/SiO_2 ratio when the mole fraction of CaO equals to 0.3 and Al_2O_3 less than 0.25 [32]. In fact, the viscosity of the slags is determined not only by DOP but also by the strength of polymerization, which is reduced by the substitution of [AlO_4] for [SiO_4] due to the instability of Al-O bonds compared with Si-O. The exceptions are therefore reasonable to some extent if we take both factors into consideration. In the present 11 studied samples, Q^4 always advantages over other Q^n species, while Q^0 and Q^1 can be neglected due to their tiny quantity. The contents of Q^2 and Q^3 exhibit a maximum value in sample CAS1 where most NBOs are observed because Ca is far beyond that required for charge compensation. Comparing **Figure 6(b)** with **(c)** it should be noted that the concentration of Q^4 in Al invariably exceeds that in Si, suggesting that Al is

preferentially localized in the more polymerized environments acting as the network intermediates, while Si is more likely to act as terminals at the network boundaries. Same results were also reported by high-energy x-ray diffraction in CAS glasses [27] and ^{29}Si NMR in Na containing aluminosilicate glasses [34].

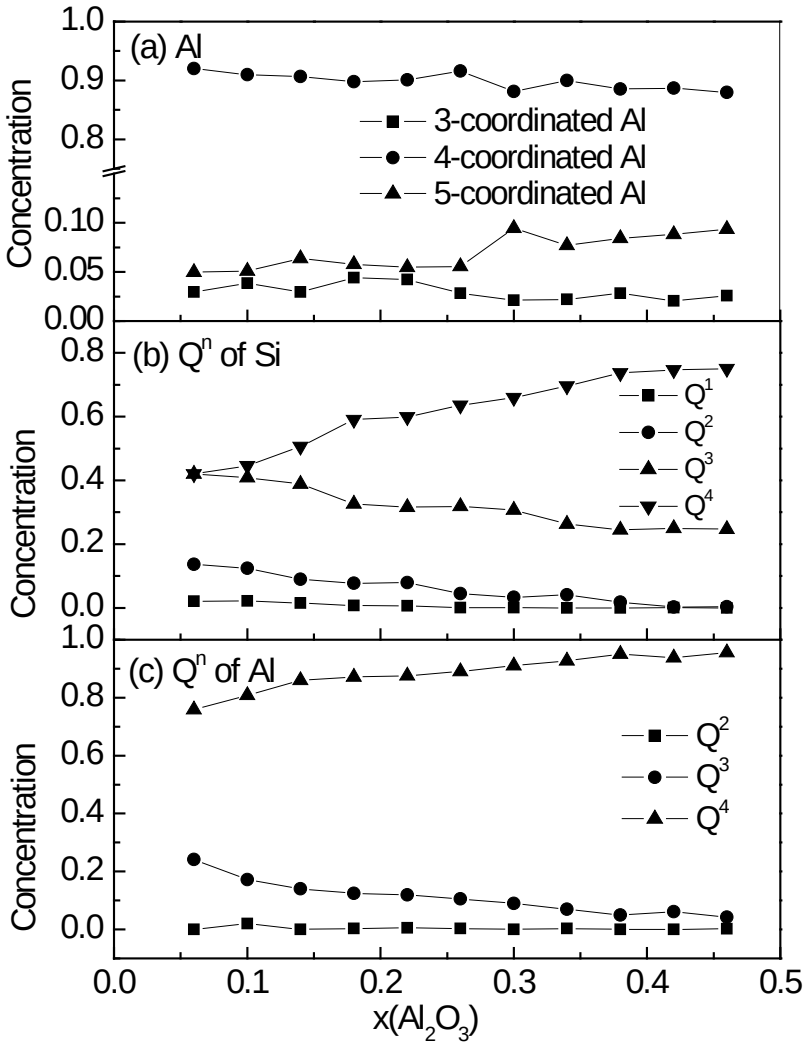

Figure 6 (a) Concentration of Al coordinated with different numbers of O, **(b)** distributions of Q^n of Si versus mole fraction of Al_2O_3; **(c)** distributions of Q^n of Al versus mole fraction of Al_2O_3

It can be concluded that the concentration of Al^V varies from 4% to 10% and its character changes from acid to alkali as the molar ratio of Al_2O_3/SiO_2 equal to the unit. The concentration of Q^4 increases dramatically at the cost of a decreasing in Q^2 and Q^3 with increasing Al_2O_3/SiO_2 ratio, indicating a high DOP of the system. Al is preferentially localized in the more polymerized environments acting as the network intermediates.

3.4 Distributions of bond lengths and bond angles

RDF offers some fundamental information about distribution of bond lengths without classification. In fact, bond lengths of Si-O and Al-O differ according to the diversity of the oxygen environments, as illustrated in **Figure 7**, and three types of Si-O distances (Si-O_{nb}, Si-O_b-Si, Si-O_b-Al) and four kinds of Al-O distances (Al-O_{nb}, Al-O_b-Si, Al-O_b-Al, Al-O_{tri}) for sample CAS7 are included. All curves are normally distributed and the height of them represents the

concentration of different types of oxygen. The sequences of the lengths are Si-O_{nb}(-Ca) < Si-O_b(-Al) < Si-O_b(-Si) and Al-O_{nb}(-Ca) < Al-O_b(-Al) < Al-O_b(-Si) < Al-O_{tri}, and this agrees well with the attractive force between O and cations (Ca < Al < Si). The third Al being coordinated to Al-O-Al influences the charge arrangement of oxygen and elongates Al-O bonds to 1.92Å in average and the less stable structure of [AlO_4] tetrahedron gives rise to a wider distribution of Al-O than that of Si-O.

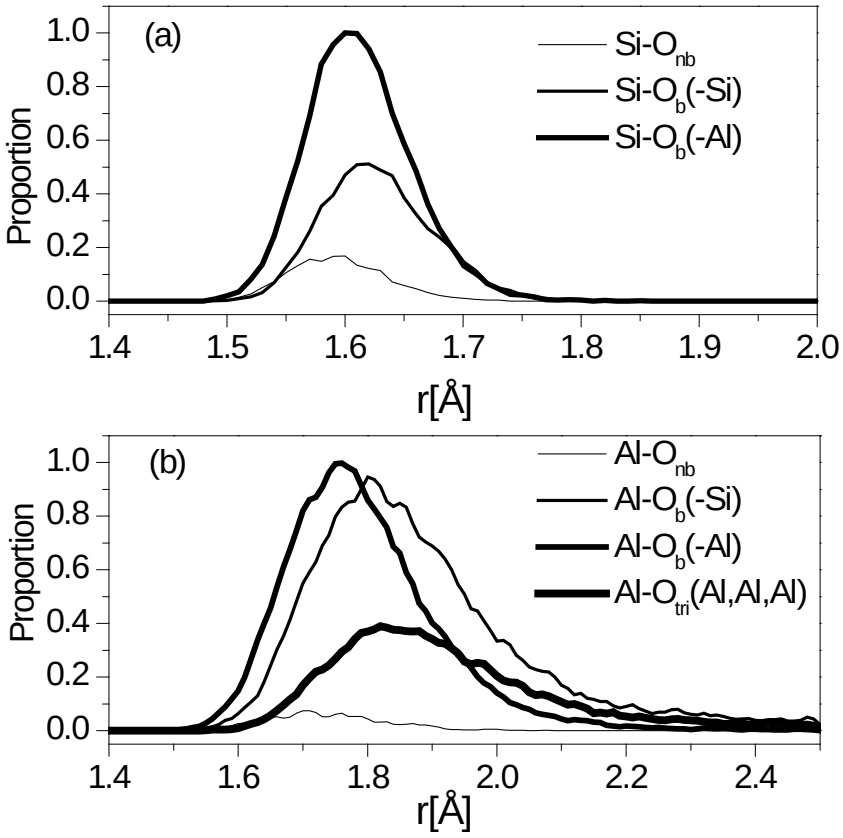

Figure 7 (a) Distributions of Si-O and **(b)** Al-O bond lengths.

The distributions of OSiO, OAlO, SiOSi, AlOAl and AlOSi angles of 5 samples are presented in **Figure 8** and **Figure 9**, respectively. The OSiO and OAlO angular distributions present a quite symmetric shape in all CAS compositions averaging at 109.3° and 108.8° respectively, which are very close to the ideal tetrahedral angle (109.5°). Just as the bond lengths show, a wider distribution of angles is also observed in OAlO than in OSiO. The angular distributions of SiOSi, AlOAl and AlOSi are somewhat noisy because of the defects in process of statistics and exhibit an asymmetric shape with the average values around 152°, 129° and 140°, respectively. The average AlOSi angle is smaller than SiOSi but larger than AlOAl, which is consistent with the tendency that the T-O-T angles increase as the average length of two bonds in T-O-T decreases [12]. It should be pointed out that the angular distributions of SiOSi for sample CAS10 and AlOAl for sample CAS2 do not present a clear maximum value as others due to the low numbers of the linkages. In the three types of angles, the average angle of AlOSi decreases obviously from 142° to 136° with an increasing Al_2O_3/SiO_2 ratio, which is attributed to the increasing interactions between modifiers' network and polymerized network [35], resulting in more triclusters coordinated with Al.

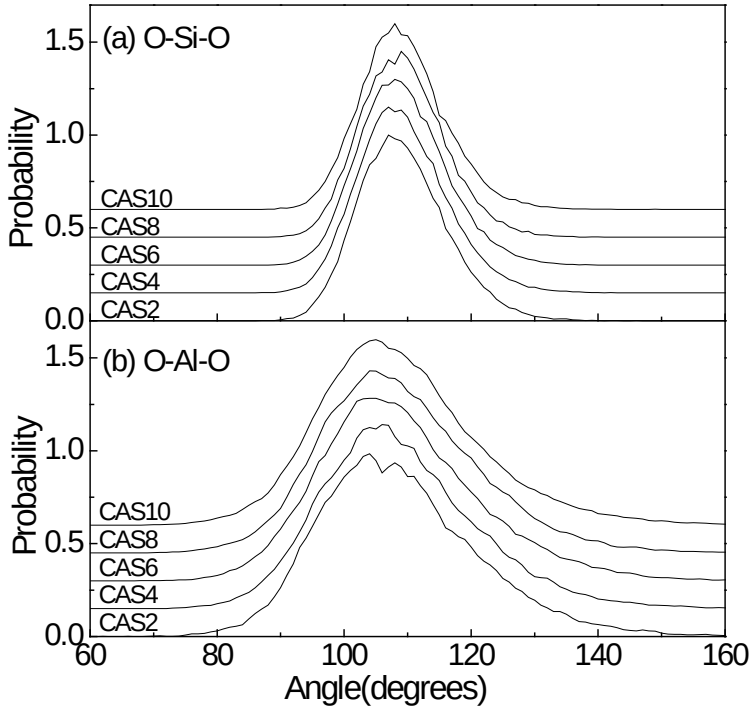

Figure 8 (a) Distributions of O-Si-O and **(b)** O-Al-O angles in tetrahedral units with varying Al_2O_3/SiO_2 ratio.

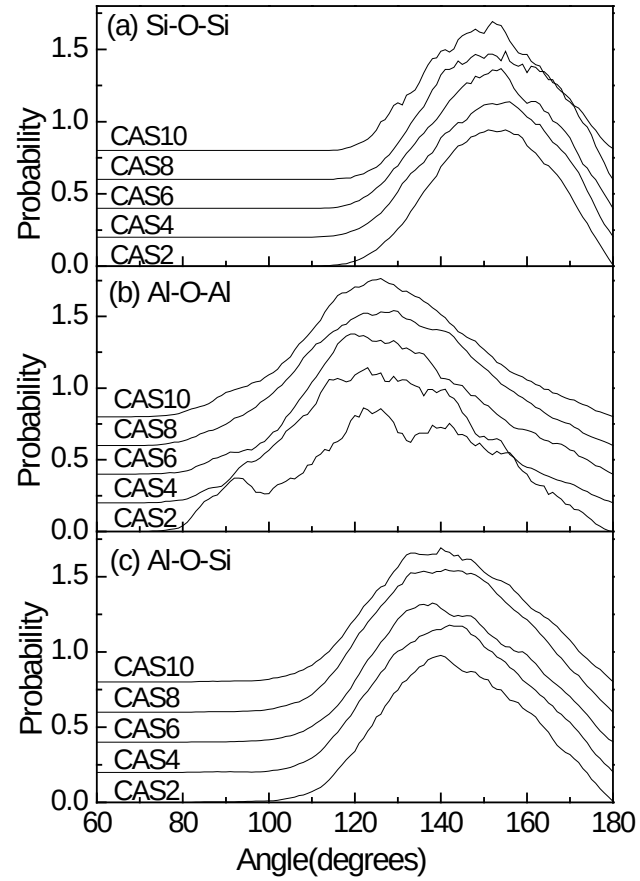

Figure 9 (a) Distributions of Si-O-Si, **(b)** Al-O-Al and **(c)** Al-O-Si with varying Al_2O_3/SiO_2 ratio.

In conclusion, the oxygen environments strongly affect the bond length of Si-O and Al-O, and further affect the distributions of bond angles, which also vary regularly with increasing Al_2O_3/SiO_2 ratio.

4. Conclusions

Molecular dynamics simulation was carried out on a series of ternary slags $CaO\text{-}SiO_2\text{-}Al_2O_3$ with different composition to study the structural properties of these systems, and the results are as follows,

(1) The substitution of Al_2O_3 for SiO_2 enhances the degree of polymerization of the slags at a fixed CaO concentration, which can be indicated from the decreasing NBOs and increasing Q^4 complexes. The viscosity of the sample may increase with increasing Al_2O_3/SiO_2 molar ratio but it is also influenced by the strength of polymerization.

(2) There is an obvious preference for NBO to be coordinated with Si while Al tends to be localized in more polymerized environment as network intermediate phases.

(3) Al avoidance principle is partially applicable especially in the silica rich regions.

(4) Oxygen triclusters are mostly composed of O(Al, Al, Al) and O(Al, Al, Si) and increase with the increasing Al_2O_3/SiO_2 ratio. The formation process is to some extent connected with that of Al^V.

(5) The distribution of bond angles interrelates with that of bond lengths and they are both influenced by the composition of slags.

Acknowledgements:

The authors wish to express their gratitude to Prof. Yongquan Wu for his help and suggestions during the simulation process. Financial supports from National Natural Science Foundation of China (50902003,51172003) and National Key Technology Research and Development Program (2010BAE00316) are gratefully acknowledged.

Reference

[1] J. R. Allwardt, S.K. Lee, J.F. Stebbins: *American Mineralogist*, **88** (2003), 949.
[2] K. Kanshashi, J.F. Stebbins: *Journal of Non-Crystalline Solids*, **353** (2007), 4001.
[3] S.K. Lee, J.F. Stebbins: *Geochimica et Cosmochimica Acta*, **70** (2006), 4275.
[4] S.K. Lee, J.F. Stebbins: *Journal of Non-Crystalline Solids*, **270** (2000), 260.
[5] Z. Wu, C. Romano, A. Marcelli, A. Mottana, G. Cibin, G. Della Ventura, G. Giuli, P. Courtial, D.B. Dingwell: *Physical Review B*, **60** (1999), 09833-1.
[6] D.R. Neuville, L. Cormier, A.-M. Flank, V. Briois, D. Massiot: *Chemical Geology*, **213** (2004), 153.
[7] L. Cormier, D.R. Neuville, G. Calas: *Journal of Non-Crystalline Solids*, **274** (2000), 110.
[8] A.C. Hannon, J.M. Parker: *Journal of Non-Crystalline Solids*, **274** (2000), 102.
[9] G.C. Jiang, J.L. You, Y.Q. Wu, H.Y. Hou, H. Chen: *Geology Geochemistry*, **31** (2003), No. 4, 0080-07.
[10] L.G. Hwa, S.L. Hwang, L.C. Liu: *Journal of Non-Crystalline Solids*, **238** (1998), 193.
[11] A. Tandia, N.T. Timofeev, J.C. Mauro, K.D. Vargheese: *Journal of Non-Crystalline Solids*, **357** (2011), 1780.
[12] L. Cormier, D. Ghaleb, D.R. Neuville, J.-M. Delaye, G. Calas: *Journal of Non-Crystalline Solids*, **332** (2003), 255.
[13] P. Ganster, M. Benoit, W. Kob, J.-M. Delaye: *Journal of Chemical Physics*, **120** (2004), 10172.
[14] L.Y. Xu, X.L. Wang, Y.Q. Wu, G.C. Jiang: *Journey of Chinese Ceramic Society*, **34** (2006), No. 9, 1117-07.
[15] J.F. Stebbins, E.V. Dubinsky, K. Kanehashi, K.E. Kelsey: *Geochimica et Cosmochimica Acta*, **72** (2008), 910.
[16] D.R. Neuville, L. Cormier, D. Massiot: *Chemical Geology*, **229** (2006), 173.
[17] M. Benoit, S. Ispas, M. Tuckerman: *Physical Review B*, **64** (2001), 224205-1.

[18] J.F. Stebbins, J.V. Oglesby, S. Kroeker: *American Mineralogist*, **86** (2001), 1307.
[19] Y.Q. Wu, G.C. Jiang, J.L. You, H.Y. Hou, H. Chen: *Journal of Central South University of Technology*, **11** (2004), 6.
[20] N.A. Morgan, F.J. Spera: *American Mineralogist*, **86** (2001), 915.
[21] D.R. Neuville, L. Cormier, V. Montouillout, D. Massiot: *Journal of Non-Crystalline Solids*, **353** (2007), 180.
[22] W. L. Wang, K. Blazek, A. Cramb: *Metallurgical and Materials Transactions B*, **39** (2008), 66.
[23] P. Courtial, D.B. Dingwell: *American Mineralogist*, **84** (1999), 465.
[24] P. Ganster, M. Benoit, J.-M. Delaye, W. Kob: *Surface Science*, **602** (2008), 114.
[25] D.R. Neuville, L. Cormier, D. de Ligny, J. Roux, A.-M. Flank, P. Lagarde: *American Mineralogist*, **93** (2008), 228.
[26] J.F. Stebbins, Z. Xu: *Nature*, **390** (1997), 60.
[27] V. Petkov, S.J.L. Billinge, S.D. Shastri, B. Himmel: *Physical Review Letters*, **85** (2000), 3436.
[28] W. Loewenstein: *American Mineralogist*, **39** (1954), 92.
[29] S.K. Lee, J.F. Stebbins: *American Mineralogist*, **84** (1999), 937.
[30] M. Schmucker, H. Schneider: *Journal of Non-Crystalline Solids*, **311** (2002), 211.
[31] X. Xue, M. Kanzaki: *Journey of Physical Chemistry B*, **103** (1999), 10816.
[32] Verein Deutscher Eisenhuttenleute (VDEh). Slag Atlas, 2nd Edition, (1995), 364.
[33] Z.T. Zhang, G.H. Wen, P. Tang, S. Sridhar: *ISIJ International*, **48** (2008), 739.
[34] H. Maekawa, T. Maekawa, K. Kawamura, T. Yokokawa: *Journal of Non-Crystalline Solids*, **127** (1991), 53.
[35] F. Angeli, J.-M. Delaye, T. Charpentiel, J.-C. Petit, D. Ghaleb, P. Faucon: *Chemical Physics Letters*, **320** (2000), 681.